

Mass-resolved two-dimensional momentum imaging of the Coulomb explosion of N_2 and SO_2 in an intense laser field

Akiyoshi Hishikawa^{a,b}, Atsushi Iwamae^{a,b}, Kennosuke Hoshina^{a,b},
Mitsuhiko Kono^{a,b}, Kaoru Yamanouchi^{a,b,*}

^a Department of Chemistry, School of Science, The University of Tokyo, 7-3-1 Hongo, Bunkyo-ku, Tokyo 113, Japan

^b Japan Science and Technology Corporation, Kawaguchi Center bldg., 4-1-8 Hon-cho, Kawaguchi, Saitama 332, Japan

Received 23 September 1997; in final form 27 October 1997

Abstract

The Coulomb explosion reactions of N_2 and SO_2 caused by the irradiation of intense laser light were investigated by high-resolution mass spectroscopy. For N_2 , from the least-squares fit to the split mass patterns for the N^+ , N^{2+} and N^{3+} channels, kinetic energy releases of six explosion pathways were determined. By rotating the laser polarization direction with respect to the detection axis, angular distributions for the singly and multiply charged atomic ion fragments were obtained and were converted to mass-resolved two-dimensional momentum imaging (MRMI) maps. This MRMI method was found to be useful to correlate ion fragments produced after the Coulomb explosion. MRMI was also applied to the Coulomb explosion of SO_2 . © 1998 Elsevier Science B.V.

1. Introduction

The advent of an ultrashort pulsed laser has enabled us to investigate a new research field of photochemistry. As Zewail [1] has demonstrated in his pioneering work, a pump-and-probe technique visualizes the nuclear motion of small molecular systems in their electronically excited state in the time domain. However, it becomes possible to generate an intense light field using the ultrashort nature of light pulses. By focusing such intense laser light the peak intensity can reach several tens of petawatt/cm² ($1 \text{ PW/cm}^2 = 10^{15} \text{ W/cm}^2$), which corresponds to the magnitudes of the Coulombic field felt by an electron in a hydrogen atom. When such a strong oscilla-

tory field interacts with molecules, an interaction between a molecule and the laser-light field cannot be treated in a perturbative manner, because it should be included as one of the dominant terms in a Hamiltonian. It has been demonstrated both theoretically and experimentally that a dressed-state picture becomes appropriate when an H_2^+ ion is exposed in an intense laser field [2,3].

The irradiation of the strong laser light onto molecules can also produce multiply charged photofragments with high kinetic energy. This phenomenon is called the Coulomb explosion in an intense laser field and has been a research target in recent years [4–25]. Codling and Frasinski [13] introduced a covariance mapping technique to correlate multiply charged fragments produced after the explosion reaction. For the Coulomb explosion of N_2

* Corresponding author.

molecules, they demonstrated that fragment ions with a certain charge number are produced from parent molecules with different charge numbers; e.g. N^+ can be formed from both N_2^{2+} and N_2^{3+} from the explosion reactions, $N_2^{2+} \rightarrow N^+ + N^+$ and $N_2^{3+} \rightarrow N^+ + N^{2+}$. For polyatomic molecules, it has also been shown that the covariance mapping technique [11,12] and its variation [14–16] are useful in correlating multiply-charged photofragments produced after the Coulomb explosion phenomenon. The angular distribution of the ejected ion fragments after the Coulomb explosion of CO was investigated by Hatherly et al. [17] and Normand et al. [18] by changing the laser polarization angle with respect to the detection axis of ion fragments and narrower angular distributions were found for ion fragments with a larger charge number.

In this Letter, we study the Coulomb explosion phenomena of N_2 and SO_2 molecules using a high-resolution time-of-flight (TOF) mass-spectroscopic technique and attempt to identify fission pathways as well as to determine kinetic energy release of the fragment ions with high precision. By rotating the laser polarization angle with respect to the detection axis of the TOF spectrometer, we determine angular distributions of the N^{z+} ($z = 1-3$) fragment ions of N_2 . For both N_2 and SO_2 , the split mass profiles, containing the information of the kinetic energy release of the ion fragments, are taken at different laser polarization angles and are converted into mass-resolved momentum imaging (MRMI) maps on a two-dimensional momentum plane.

2. Experimental

Femtosecond laser pulses at 795 nm, with a typical pulse duration of 52 fs, were generated by a mode-locked Ti-sapphire laser (Spectra-Physics Tsunami) which was pumped by a frequency-doubled output of a diode-laser-pumped Nd:YVO₄ laser (Spectra-Physics Millennia). The output of the Tsunami was introduced to a regenerative amplifier system (BM-Industry Alpha 10B/S), in which the two sequential bow-tie amplifier stages were used to amplify the output of a regenerative amplifier, to obtain high-power low-repetition rate (10 Hz) short-pulsed laser light. After the pulse compressor, the

duration of the amplified laser pulse was 100 fs, measured by an auto-correlator (MC2 Femtoscope) and the total energy reached as high as 50 mJ/pulse.

The light beam was focused by a quartz lens ($f = 152$ mm at 795 nm) onto a pulsed molecular beam between the extraction parallel plates of a linear time-of-flight (TOF) mass spectrometer (Jordan Linear-TOF) with a flight length of 1400 mm. The singly and multiply charged atomic and molecular ions produced after the Coulomb explosion were detected by a multichannel-plate (MCP) detector placed at the end of the flight tube. Typical mass resolution of $m/\Delta m \sim 620$ was achieved, which was found to be high enough to resolve the same ion fragments produced from different multiply-charged states of a parent diatomic molecule. The TOF mass spectra were recorded by a digital oscilloscope (LeCroy 9370) with a 1 GHz sampling rate.

In deriving the mass-resolved two-dimensional momentum imaging map, a zero-order half-wave plate (CVI) was introduced after the compressor stage of the Alpha-10 system in order to rotate the laser polarization direction with respect to the detection axis of the TOF mass spectrometer. The half-wave plate was rotated manually with an angle interval of 6°, which corresponds to a polarization angle interval of 12°. In total 15 high-resolution TOF spectra were taken to construct the MRMI map. Since an axial symmetry is expected around the direction of the polarization vector, information obtained from the angles between 180° and 90° should be the same as that from the angles between 0° and 90°. However, the MRMI patterns were constructed using all 15 spectra covering the 180° rotation angle. Since a symmetrical MRMI pattern with respect to the line connecting the 0° and 180° positions is expected, the degree of asymmetry in the observed MRMI pattern was used as diagnostics of the variation of the experimental conditions during the repetitive TOF data acquisition. The TOF signals for a charged state of atomic or diatomic fragments, exhibiting a structure associated with their different kinetic energies, was converted to a momentum distribution to compare it with those obtained for different fragment-ion channels.

By assuming a Gaussian spatial profile, the spot size of the laser beam at the molecular beam was estimated to be 13 μm in diameter. This means that

the laser intensity at the molecular beam is 7 PW/cm² when the output of the regenerative amplifier system is 1 mJ/pulse. The sample gas (N₂ or SO₂) was introduced into a high vacuum chamber (1.2 × 10⁻⁸ Torr) through a pulsed valve. After passing through a skimmer, a molecular beam was introduced into the laser-molecule interaction region. During the experiment, the pressure in the main chamber was kept sufficiently low (< 1 × 10⁻⁷ Torr) in order to avoid the space charge effect [6].

3. Coulomb explosion of N₂

3.1. Explosion patterns at fixed polarization

When the laser polarization was set parallel to the TOF detection axis, all the mass peaks of nitrogen atom ions, N⁺, N²⁺ and N³⁺, in our TOF mass spectrum at 3.5 PW/cm² split to form a doublet as seen in Fig. 1. These doublets mean that the atomic ions produced travelled first in forward and backward directions and the forward fragments were accelerated further than the backward fragments which must be decelerated first and then change direction and be accelerated, causing a flight time difference between the two types of fragments. The

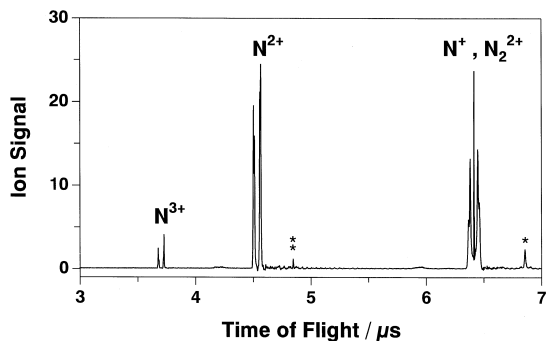


Fig. 1. The time-of-flight spectrum of N₂ recorded when N₂ was irradiated with intense laser light (3.5 PW/cm²) at λ = 795 nm with the laser polarization direction parallel to the TOF spectrometer axis. The pressure in the main chamber was 9.2 × 10⁻⁸ Torr and the electric field at the extraction region was 298 V/cm. Doublet structures are clearly identified for the three ion species, N⁺, N²⁺ and N³⁺, which result from the forward and backward recoiled components. The small peak marked with an asterisk and that with two asterisks are the O⁺ and O²⁺ signals produced from H₂O, respectively.

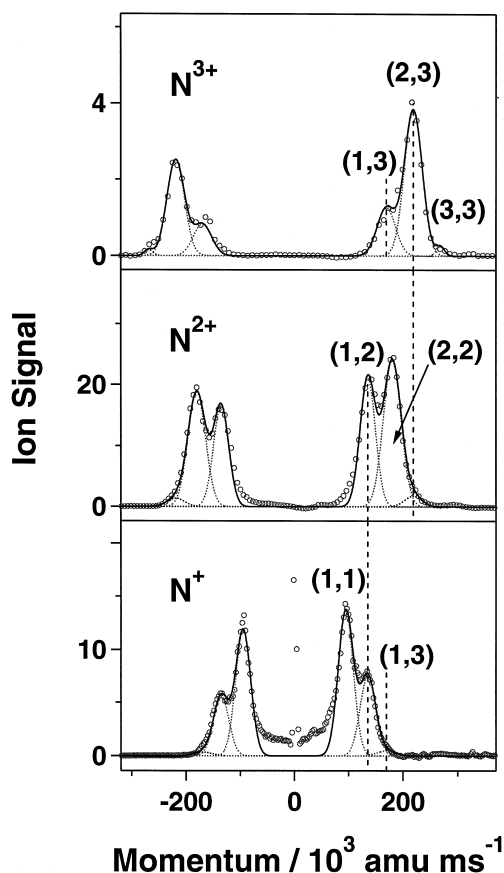


Fig. 2. The experimental time of flight spectra of N⁺, N²⁺ and N³⁺ in Fig. 1 plotted as a function of a momentum of the fragment ion (open circle). Three components, attributable to different explosion pathways, are seen in all the channels. The assignment of the explosion pathways, N₂ⁿ⁺ → N^{p+} + N^{q+}, are denoted as (p, q). The result of the multiple-Gaussian least-squares fit is shown (solid curve) with the three components used in the fit (dotted curve). The ordinate represents the signal output of the MCP detector. The dependence of the collection efficiency of the fragment ions on their initial momenta is not corrected.

kinetic energy release of the fragment pathway, N₂ⁿ⁺ → N^{p+} + N^{q+} (n = p + q), referred to as the (p, q) pathway hereafter was obtained from the time separation of the doublet peaks in the TOF spectrum. It has also been known that the critical bond distance r_c, at which the Coulomb repulsion energy is released to form fast fragment ions, can also be calculated from the kinetic energy release [26].

From the high-resolution TOF spectrum, it becomes possible to identify different fragment path-

ways with different kinetic energy releases. In Fig. 2, the doublet peaks identified for the N^+ , N^{2+} and N^{3+} channels in Fig. 1 were expanded and scaled linearly with respect to the momentum imposed on the atomic fragment. It was found that all the three channels exhibited a partially split double-peak structure with a shoulder on the higher kinetic energy side in both the forward and backward peaks, indicating the existence of at least three Coulomb explosion pathways.

When the Coulomb explosion occurs, starting from multiply charged parent ions $N_2^{n+} \rightarrow N^{p+} + N^{q+}$, equal amounts of the momentum are imposed on both atomic fragments. Therefore, by comparing the N^{2+} channel with the other N^+ and N^{3+} channels in Fig. 2, the counterpart atomic fragments associated with the three components in the N^{2+} channel can be identified. The lowest momentum peak among the three components in the N^{2+} channel is formed with the N^+ channel and the highest momentum peak is formed with the N^{3+} channel. Consequently, the center peak in the three components forms two N^{2+} fragments. It can be concluded that the three pathways, (1,2), (2,2) and (2,3), produce the N^{2+} fragment ion with different momenta.

In a similar manner to the N^{2+} channel, the (1,1) pathway is identified in the N^+ channel in addition to the (1,2) pathway. On the lower kinetic energy side of these two pathways, a weak tail extending towards the lower kinetic energy region can be identified. This tail part was assigned to a neutral pathway (0,1), with a much smaller kinetic energy release than the Coulomb explosion pathways. The sharp centered peak in the N^+ channel is assigned to the doubly charged parent ions, N_2^{2+} , which has the same m/q as N^+ . These assignments are consistent with previous ones obtained by TOF [6,7] and covariance [4,8–10] measurements.

In the N^{3+} channel, the (1,3) pathway is clearly identified in addition to the (2,3) and (3,3) pathways as assigned in Fig. 2. In the N^+ channel, there is a weak profile assignable to the (1,3) pathway as shown in this figure. Previously, Cornaggia et al. [7] reported that there is a (1,3) pathway. Later, the existence of the (1,3) pathway was denied by Codling et al. [10] because a clear correlation was not found for the (1,3) pathway in their covariance map. However, in our TOF mass spectrum, thanks to the

high-resolving power, the (1,3) pathway, in which charges are distributed to the two fragment ions in an asymmetrical way, was identified. This asymmetrical charge distribution cannot be explained by the Thomas–Fermi–Dirac model [19] and may be regarded as evidence of charge localization [23,24].

By assuming a Gaussian profile in the momentum distribution of the atomic fragments, the least-squares fit to the partially resolved structure of all the three N^+ , N^{2+} and N^{3+} ion channels was performed and absolute values of the momentum, defined as the centers of the Gaussian profiles, were determined with high-precision. In the least-squares fit, a constraint was imposed so that a pathway commonly observed in different fragment channels has the same kinetic energy release and the same momentum distribution in those channels. Such pathways are (1,2) in the N^+ and N^{2+} channels, (1,3) in the N^+ and N^{3+} channels and (2,3) in the N^{2+} and N^{3+} channels.

If we assign a single Gaussian type profile to represent the (1,0) pathway in the tail region of the N^+ channel on its low-energy side, it could have a wide momentum distribution covering the (1,1) and (1,2) regions. However, since it is expected that the (1,0) pathway has substantially lower kinetic energy release than the (1,1) and (1,2) pathways, its momentum distribution may not extend into the (1,1) and (1,2) regions. Therefore, a single Gaussian profile may not be appropriate to represent the momentum distribution of this weak neutral pathway. In conse-

Table 1

The kinetic release energies and momenta in the Coulomb explosion reaction of N_2 in the intense laser field (3.5 PW/cm²) determined by the least-squares fit to the high resolution TOF mass spectrum^a

Fragmentation pathway	Release energy (eV)	Momentum (10 ³ amu ms ⁻¹)
$N^+ + N^+$	6.6 (1)	94.5 (9)
$N^+ + N^{2+}$	13.6 (2)	135 (2)
$N^+ + N^{3+}$	22 (7)	170 (30)
$N^{2+} + N^{2+}$	24.2 (3)	181 (1)
$N^{2+} + N^{3+}$	36 (2)	219 (9)
$N^{3+} + N^{3+}$	56 (1) ^b	276 (2) ^b

^aIn the TOF mass spectrum, the dependence of the collection efficiency of the fragment ions on their initial momenta was not corrected.^bObtained at 9.6 PW/cm².

quence, only the (1,1) and (1,2) pathways are considered in the least-squares fit of the N^+ channel and the momentum data smaller than $70 \times 10^3 \text{ amu m s}^{-1}$ was not included in the fit. Similarly, in order to decrease the influence of the neutral pathway in the N^{2+} channel, the momentum data of the N^{2+} channel smaller than $110 \times 10^3 \text{ amu m s}^{-1}$ were not included in the fit. The least-squares fits to the observed profiles were performed with only small residuals as shown in Fig. 2 and the momentum values and the released kinetic energies for the six pathways (1,1), (1,2), (1,3), (2,2), (2,3) and (3,3), were determined with high-precision as listed in Table 1.

The observed width of the momentum distribution of the atomic fragments has a contribution from: (i) the distribution of the momentum transferred after the Coulomb explosion, (ii) the initial momentum distribution of the parent molecules at room temperature and (iii) the limited velocity resolution, determined by the diameter of the MCP detector. Our successful fit of the momentum distributions of the fragment ion channels described above, indicates that the Gaussian profiles are appropriate for representing the mixture of these three contributions.

3.2. MRMI patterns

The mass-resolved momentum imaging maps for the Coulomb explosion of N_2 were obtained by rotating the laser polarization in a stepwise manner. In Fig. 3, contour plots of the imaging pictures for the N^+ , N^{2+} and N^{3+} channels are displayed on a two-dimensional momentum plane. It should be noted that the shape of the cross section along the vertical and horizontal axes in the imaging pictures corresponds to the mass-split pattern obtained when the laser polarization direction is parallel and perpendicular to the TOF detection axis, respectively.

The angular and the velocity resolution in the MRMI map was limited by the finite area of the MCP detector ($d = 18 \text{ mm } \varnothing$) located 1400 mm downstream from the laser-molecule interaction region. The effective acceptance angle 2δ , which can be used as a measure of the angular resolution, may be given by $\delta \sim d/(2\Delta t v_0)$, where t and v_0 denote the flight time and the velocity of the fragment ions, respectively. Though the effective acceptance angle tends to become smaller for the ion fragments with faster velocity, it falls to $\delta \sim 10^\circ$ in most cases, which is comparable with the interval (12°) of the

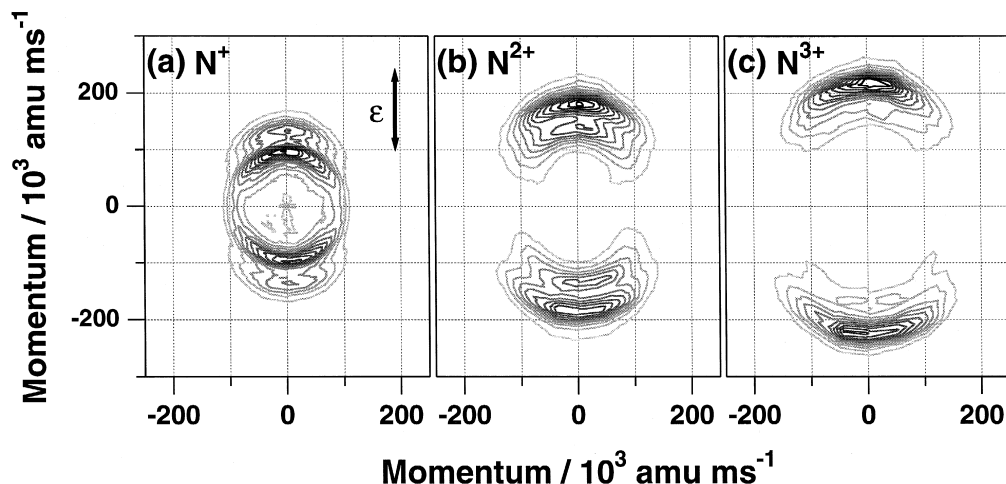


Fig. 3. The mass-resolved momentum imaging (MRMI) maps of N_2 at 3.5 PW/cm^2 for the (a) N^+ , (b) N^{2+} and (c) N^{3+} channels. It is clearly seen that the angular distribution of the higher ionized fragments becomes narrower. The scale of the intensity contour of each picture is normalized by the most intense peak, whose intensity is 1, 2.7 and 0.50 in a relative scale for the N^+ , N^{2+} and N^{3+} channels, respectively. The vertical arrow in (a) represents the direction of the laser polarization vector.

polarization angle. For example, the acceptance angles for the N^{2+} and N^{3+} fragments for the (2,3) pathway becomes $\delta \sim 9^\circ$, while that for the N^+ fragments for the (1,1) pathway is 12° . The velocity resolution may be expressed as $\Delta v/v \sim (1/8)d^2/(v_0\Delta t)^2$. For the N^+ , N^{2+} and N^{3+} fragments, a velocity resolution smaller than $\Delta v/v = 10\%$ can be attained when the momentum exceeds 44×10^3 , 63×10^3 and 76×10^3 amu m s⁻¹, respectively.

As clearly seen in the crescent-shaped domains in the three imagings, the momentum of the charged atomic fragments increases as the charge number of the fragment increases and the angle spanned by the arc along the crescent-shaped distribution tends to become smaller. The increase of the momentum reflects the fact that larger kinetic energies are released after the Coulomb explosion when the charge number of the parent N_2^{n+} ion becomes larger. The decrease of the angle spanned by the arc reflects the fact that the extent of the alignment of the N–N molecular axis along the laser polarization becomes larger for the higher charged parent ions.

This alignment effect was quantitatively evaluated by fitting the intensity at a constant momentum along the circle on which the most intense peak at the parallel polarization configuration is ($\theta = 0$), as a functional of the form $\cos^k\theta$, where θ is a polarization angle and k is a variable parameter. For the (1,1), (2,2) and (2,3) pathways, the optimized k values are 2.8(3), 6.0(5) and 7.0(5), respectively. If we evaluate this angular distribution as a full-width at half-maximum (FWHM) of the $\cos^k\theta$ distribution, the FWHMs become $76(6)^\circ$, $54(5)^\circ$ and $45(4)^\circ$, respectively. When the light intensity becomes larger, a higher degree of alignment is expected and simultaneously the number of higher charged parent ions is expected to increase. The observation that the extent of the alignment becomes larger for the higher charged parent ions may be ascribed to the spatial distribution of the laser intensity. Even though we have a small focal spot of the laser ($13 \mu\text{m}$ \emptyset), a higher-degree of alignment is achieved and the higher charged fragments are produced in a spatial region closer to the center of the laser spot with a stronger intensity.

In the N^+ channel, outside the clear crescent-shaped area, a less pronounced crescent can be seen.

When we compare this imaging figure with the mass-pattern in the N^+ channel in Fig. 2, the assignment of these areas is straightforward. The inner and outer crescent-shaped regions correspond to the (1,1) and (1,2) pathways. This kind of inner and outer crescent structure can also be seen in the MRMI picture of the N^{2+} channel. When we compare MRMI patterns of the N^+ and N^{2+} channels in Fig. 3, expressed with the same momentum scale, the area of the outer crescent in the N^+ channel almost overlaps with the inner crescent in the N^{2+} channel. Considering the discussion in Subsection 3.1, this means that the momentum distributions of the N^+ and N^{2+} coincide with each other and both of the distributions are assigned as the contribution from the (1,2) pathway. As has been demonstrated here, one of the advantages of the MRMI method is that the correlation between multiply charged fragments is identified securely by comparing corresponding two-dimensional momentum areas with information on both momentum and angular distributions of the fragment ions.

4. Coulomb explosion of SO_2

The investigation of the Coulomb explosion phenomena has been extended to polyatomic molecules by Frasninski and co-workers [11,12] and Cornaggia and co-workers [14–16]. Cornaggia [16] reported the Coulomb explosion process of CO_2 using a double-correlation map, which can be regarded as a variation of the covariance map introduced by Frasninski and co-workers [4,13], and argued that a large amplitude bending motion occurs during the Coulomb explosion. Furthermore, they investigated the Coulomb explosion of SO_2 [15] and inferred the possibility of taking a linearly averaged geometry for the highly charged channels $\text{O}^{2+} + \text{S}^{3+} + \text{O}^{z+}$ ($z = 1-3$) channels. From a comparison of the double-correlation maps for the $\text{O}^+ + \text{C}^+ + \text{O}^{z+}$ ($z = 1,2$) pathways of CO_2 and the corresponding $\text{O}^+ + \text{S}^+ + \text{O}^{z+}$ ($z = 1,2$) pathways of SO_2 , they suggested that the fission pathways are influenced not only by the electron configuration of the multiply charged parent ions but by the initial geometrical structure. In order to demonstrate the applicability of our MRMI method

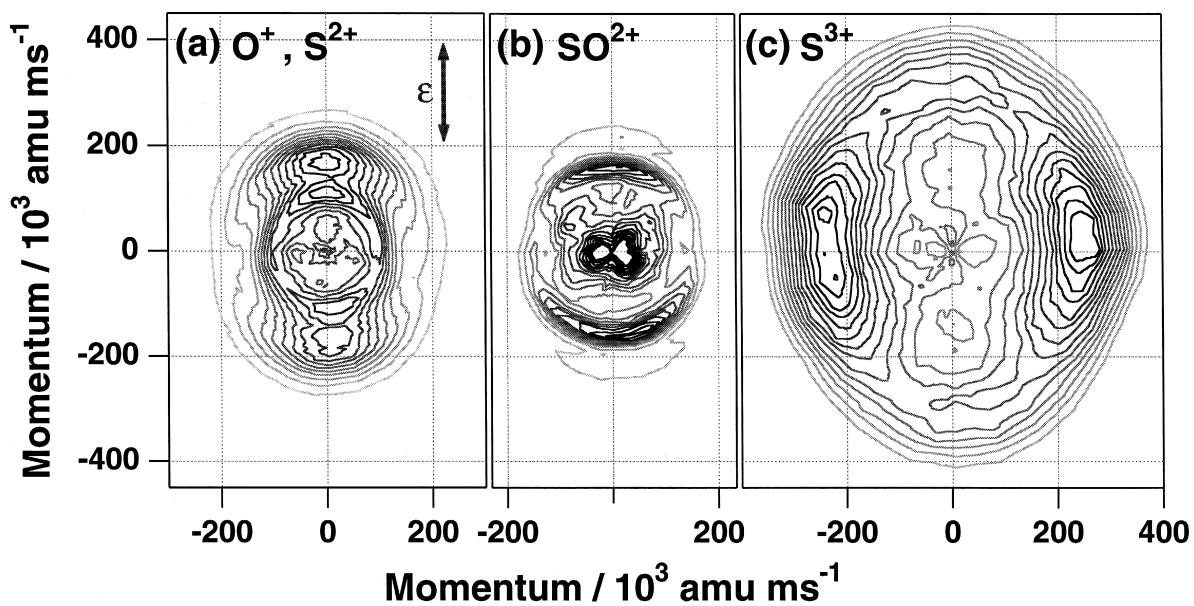


Fig. 4. The MRMI maps of SO_2 at 5.4 PW/cm^2 with the main chamber pressure of 1.5×10^{-7} Torr and the extraction electric field of 299 V/cm . The vertical arrow in (a) represents the direction of the laser polarization vector. (a) O^+/S^{2+} channel: two pairs of crescents are visible in the polarization direction which result mostly from the three body explosion of SO_2 and is also partly attributed to the $\text{SO}_2^{2+} \rightarrow \text{SO}^+ + \text{O}^+$ and $\text{SO}_2^{3+} \rightarrow \text{SO}^{2+} + \text{O}^+$ pathways. (b) SO^{2+} channel: a pair of the crescents located in the polarization direction represents the $\text{SO}_2^{3+} \rightarrow \text{SO}^{2+} + \text{O}^+$ explosion pathway, while the slow release energy component in the central region is attributed to the neutral pathway, $\text{SO}_2^{3+} \rightarrow \text{SO}^{2+} + \text{O}$. (c) S^{3+} channel: a pair of prominent crescents is observed in the direction perpendicular to the laser polarization, indicating that the critical geometry prior to the Coulomb explosion takes a bent form (see text). The intensity scale in these maps is normalized by the most intense peak in the respective channels, whose intensities are 1, 0.09 and 0.55 in a relative scale for the O^+/S^{2+} , SO^{2+} and S^{3+} channels, respectively.

to a triatomic system, we investigate the Coulomb explosion of SO_2 .

We recorded the TOF spectrum of SO_2 with a typical laser intensity of 5.4 PW/cm^2 . In Fig. 4, the MRMI maps of three different mass channels are shown. In Fig. 4(a), two fragment channels of S^{2+} and O^+ , with the same m/q values, are observed at the same flight time. Along the vertical axis, there are two prominent peaks, forming an inner thin crescent and an outer thick crescent in the two dimensional momentum plane. On the basis of the double-correlation map of SO_2 reported by Cornaglia et al. [15], both of the crescents can be assigned to the O^{2+} channel, indicating that the principal a -axis of SO_2 , along which the largest dynamical polarizability is expected, is aligned strongly along the laser polarization and the oxygen atoms on both ends of the molecules are ejected with a large momentum towards the direction parallel with the laser

polarization. Near the horizontal direction the upper and lower inner crescent merge and they form a circular rim in the two dimensional plane. Along the horizontal direction, there are two peaks corresponding with the right and left ridges of the circular rim. These two peaks may represent the contribution from the S^{2+} channels, which may eject S^{2+} in a direction perpendicular to the laser polarization.

When we compare the MRMI plot of the SO^{2+} channel displayed in Fig. 4(b) with Fig. 4(a), both of which are drawn with the same momentum scale, the crescent in (b) covers the inner side of the outer crescent in (a). Therefore, it can be said that the inner part of the outer crescent in (a) contains the $\text{SO}^{2+} + \text{O}^+$ fragmentation pathway. Similarly, the crescent-shaped area in the MRMI plot of the SO^+ channels, which is not drawn here, covers an area of the inner side of the inner crescent in (a), indicating the contribution from the fragmentation pathway of

$\text{SO}^+ + \text{O}^+$. These diatomic-ion formation pathways were identified first by Cornaggia et al. [15] based on their double correlation map.

From the relative intensity of the different mass channels, the contribution from the diatomic-ion formation pathways with respect to the three body fission pathways can be evaluated. It was found that their abundances are relatively small ($\sim 15\%$ for the SO^+ pathway and $\sim 7\%$ for the SO^{2+} pathway) compared with those for the three body fission pathways, but they are large enough to form a peak in the MRMI maps. It should be noted that the overall feature of the two pairs of the thick crescent-shaped areas in Fig. 4(a) is constructed by the dominant three-body fragmentation pathways.

In Fig. 4(c), the S^{3+} channel is shown, whose MRMI pattern is different from the previous ones. Two prominent crescent-shaped areas are found in the direction perpendicular to the laser polarization. Since the molecular a -axis of the SO_2 is expected to be highly aligned along the laser polarization direction, this distribution of the S^{3+} fragment indicates that the S^{3+} is ejected with a large momentum in a perpendicular direction to the laser polarization, indicating that the Coulomb explosion reaction occurs from the bent geometrical structure.

If we assume that the dominant Coulomb explosion pathways to form S^{3+} are symmetric ones, i.e. $\text{SO}_2^{(3+2q)+} \rightarrow \text{O}^{q+} + \text{S}^{3+} + \text{O}^{q+}$ and that the charge difference $|q - 3|$ is smaller than or equal to 2, i.e. $|q - 3| \leq 2$, five symmetric pathways for $q = 1-5$ are possible. In our experimental conditions, the yields of the O^{3+} , O^{4+} and O^{5+} channels are significantly smaller ($< 15\%$) than the S^{3+} yield. Therefore, we consider only two channels for $q = 1$ and 2. Once the fragmentation pattern is known, the critical geometrical structure of the highly charged parent ion at which the Coulomb explosion occurs can be derived. The critical O–S–O angle γ_c , which is approximated as an angle between the two momentum vectors of the O^{q+} fragments, is expressed as $\gamma_c = 2 \tan^{-1}(2p(\text{O}^{q+})/p(\text{S}^{3+}))$, where $p(\text{O}^{q+})$ represents the component of the momentum of O^{q+} parallel with the laser polarization direction and $p(\text{S}^{3+})$ the total momentum of S^{3+} . From the two main peaks in the MRMI map in Fig. 4(c), $p(\text{S}^{3+}) = 240 \times 10^3 \text{ amu m s}^{-1}$ and from the MRMI map for O^{2+} , $p(\text{O}^{2+}) = 257 \times 10^3 \text{ amu m s}^{-1}$. By using

these two data, γ_c for the $q = 2$ pathway was determined to be $\gamma_c = 130$. From the momenta of these fragments, the total released kinetic energy $E_{\text{total}}(q)$ for the $q = 2$ channel was calculated to be $E_{\text{total}}(2) = 61.5 \text{ eV}$. If simple Coulombic potentials are adopted for the three fragment ions, $\text{O}^{2+} + \text{S}^{3+} + \text{O}^{2+}$, the critical bond length $r_c(\text{S–O})$, at which the Coulomb explosion occurs, can be expressed as $r_c(\text{S–O}) = 204.6/E_{\text{total}}(2) = 3.3 \text{ \AA}$. For the $q = 1$ pathway, $\gamma_c = 110$ and $r_c(\text{S–O}) = 2.5$ were derived in a similar manner as described above using $p(\text{O}^+) = 170 \times 10^3 \text{ amu m s}^{-1}$, which was derived from the MRMI map in Fig. 4(a).

For both Coulomb explosion pathways starting from SO_2^{7+} ($q = 2$) and SO_2^{5+} ($q = 1$), the γ_c values are not largely different from the equilibrium angle $\gamma_e = 119.5^\circ$ [27] of the electronic ground state of neutral SO_2 , though their uncertainties are relatively large, reflecting the broad momentum distributions shown in the MRMI maps. However, the stretch of the bond length from the equilibrium bond distance $r_e(\text{S–O}) = 1.432$ [27] is significant. For $q = 1$ and 2, $r_c(\text{S–O})/r_e(\text{S–O}) = 1.7$ and 2.3, respectively. This means that the S–O bonds in SO_2 stretch significantly before the Coulomb explosion occurs, in a similar manner to N_2 and other diatomic molecules investigated previously [19,23,24,26]. This kind of large geometrical change of a triatomic molecule was reported by Cornaggia [16], who determined $r_c(\text{C–O})/r_e(\text{C–O}) \sim 2$ for the Coulomb explosion of CO_2 . For SO_2 , Cornaggia et al. [15] argued that the molecule keeps a memory of its bent structure, even though electrons in a molecular orbital responsible for the bent geometry are considered to be ejected. Our finding, that the bent geometry of SO_2 is kept before the Coulomb explosion event for highly charged parent states such as SO_2^{5+} and SO_2^{7+} , is consistent with the remark by Cornaggia et al. [15]. Further analyses of the MRMI patterns of SO_2 will be reported in a future publication.

5. Concluding remarks

We have demonstrated that this new MRMI technique is promising to investigate the Coulomb explosion processes of small molecules. Imaging techniques have been used to visualize the angular distri-

bution of the photofragments produced after the photodissociation [28–31] and are regarded as being useful to investigate the mechanism of photodissociation processes. In the case of the Coulomb explosion of molecules, a number of fragment ions were ejected from the multiply charged parent ions almost at the same time and therefore, a technique for mass-selection should be combined in order to construct such an image. In the present study, we introduced the MRMI procedure which enabled us to obtain straightforwardly an angular map for individual ion fragment species.

The Coulomb explosion phenomena for N_2 and SO_2 were also observed in the single photon impact [32,33] and electron impact [34,35] experiments. It is expected that the results of these experiments afford us complementary information regarding the bond fission mechanism of multiply charged parent ions.

Acknowledgements

The present work has been supported by the CREST (Core Research for Evolutionary Science and Technology) fund from the Japan Science and Technology Corporation. Authors would like to mention previous pioneering studies conducted by Frasiniski, Codling and their coworkers and Cornaggia, Normand and their coworkers, which stimulated the authors interest towards the Coulomb explosion phenomena of small molecules.

References

- [1] A.H. Zewail, *Femtochemistry*, vols. I and II, World Scientific, Singapore, 1994.
- [2] A. Giusti-Suzor, F.H. Mies, L.F. Dimauro, E. Charron, B. Yang, *J. Phys. B* 27 (1994) 1.
- [3] S. Chelkowski, A. Conjusteau, T. Zuo, A.D. Bandauk, *Phys. Rev. A* 54 (1996) 3235.
- [4] L.J. Frasiniski, K. Codling, P.A. Hatherly, *Phys. Lett. A* 142 (1989) 499.
- [5] K. Codling, L.J. Frasiniski, P.A. Hatherly, M. Stankiewicz, *Phys. Scr.* 41 (1990) 433.
- [6] C. Cornaggia, J. Lavancier, D. Normand, J. Morellec, H.X. Liu, *Phys. Rev. A* 42 (1990) 5464.
- [7] C. Cornaggia, J. Lavancier, D. Normand, J. Morellec, P. Agostini, J.P. Chambaret, A. Antonetti, *Phys. Rev. A* 44 (1991) 4499.
- [8] C. Cornaggia, D. Normand, J. Morellec, *J. Phys. B* 25 (1992) L415.
- [9] M. Stankiewicz, L.J. Frasiniski, G.M. Cross, P.A. Hatherly, K. Codling, A.J. Langley, W. Shaikh, *J. Phys. B* 26 (1993) 2619.
- [10] K. Codling, C. Cornaggia, L.J. Frasiniski, P.A. Hatherly, J. Morellec, D. Normand, *J. Phys. B* 24 (1991) L593.
- [11] L.J. Frasiniski, K. Codling, P. Hatherly, *Science* 46 (1989) 1029.
- [12] L.J. Frasiniski, P. Hatherly, K. Codling, *Phys. Lett. A* 156 (1991) L307.
- [13] K. Codling, L.J. Frasiniski, *J. Phys. B* 26 (1993) 783.
- [14] C. Cornaggia, M. Schmidt, D. Normand, *J. Phys. B* 76 (1994) L123.
- [15] C. Cornaggia, F. Salin, C.L. Blanc, *J. Phys. B* 29 (1996) L749.
- [16] C. Cornaggia, *Phys. Rev. A* 54 (1996) R2555.
- [17] P.A. Hatherly, L.J. Frasiniski, K. Codling, A.J. Langley, W. Shaikh, *J. Phys. B* 23 (1990) L291.
- [18] D. Normand, L.A. Lampre, C. Cornaggia, *J. Phys. B* 25 (1992) L497.
- [19] M. Brewczyk, L.J. Frasiniski, *J. Phys. B* 24 (1991) L307.
- [20] B. Sheehy, B. Walker, L.F. Dimauro, *Phys. Rev. Lett.* 74 (1995) 4799.
- [21] B. Sheehy, L.F. Dimauro, *Ann. Rev. Phys. Chem.* 47 (1996) 463.
- [22] H. Stapelfeldt, H. Sakai, E. Constant, P.B. Corkum, *Phys. Rev. A* 55 (1997) R3319.
- [23] T. Seideman, M.Y. Ivanov, P.B. Corkum, *Phys. Rev. Lett.* 75 (1995) 2819.
- [24] M. Ivanov, T. Seideman, P. Corkum, F. Ilkov, P. Dietrich, *Phys. Rev. A* 54 (1996) 1541.
- [25] T. Seideman, M.Y. Ivanov, P.B. Corkum, *Chem. Phys. Lett.* 252 (1996) 181.
- [26] J.H. Posthumus, L.J. Frasiniski, A.J. Giles, K. Codling, *J. Phys. B* 28 (1995) L349.
- [27] Y. Morino, Y. Kikuchi, S. Saito, E. Hirota, *J. Mol. Spectrosc.* 13 (1964) 95.
- [28] P.W. Chandler, P.L. Houston, *J. Chem. Phys.* 87 (1987) 1445.
- [29] T. Kinugawa, T. Arikawa, *J. Chem. Phys.* 96 (1992) 4801.
- [30] T. Suzuki, K. Tonokura, L.S. Bontuyan, N. Hashimoto, *J. Phys. Chem.* 98 (1994) 13447.
- [31] Y. Sato, Y. Matsumi, M. Kawasaki, K. Tsukiyama, R. Bersohn, *J. Phys. Chem.* 99 (1995) 16307.
- [32] N. Saito, I. Suzuki, *Phys. Rev. Lett.* 61 (1988) 2740.
- [33] S. Hsieh, J.H.D. Eland, *Rapid Commun. Mass Spectr.* 9 (1995) 1261.
- [34] M. Lundqvist, D. Edvardsson, P. Baltzer, B. Wannberg, *J. Phys. B* 29 (1996) 1489.
- [35] D.A. Hagan, J.H.D. Eland, *Rapid Commun. Mass Spectr.* 3 (1989) 186.